bioRxiv preprint doi: https://doi.org/10.1101/2022.12.21.521364; this version posted December 21, 2022. The copyright holder for this preprint (which was not certified by peer review) is the author/funder, who has granted bioRxiv a license to display the preprint in perpetuity. It is made available under aCC-BY-NC 4.0 International license.

Short article

High-resolution glucose fate-mapping reveals *LDHB*-dependent lactate production by human pancreatic β cells

Federica Cuozzo[1], Daniela Nasteska[1], Zicong Jiao[1], Hannah R. Smith[1], Caroline Bonner[2], Julie Kerr-Conte[2], Francois Pattou[2], Rita Nano[3,4], Lorenzo Piemonti[3,4], Jennie Roberts[1], Gareth G. Lavery[1,5], Ildem Akerman[1] .Daniel A. Tennant[1*], Christian Ludwig[1*] and David J. Hodson[1,6*]

[1]Institute of Metabolism and Systems Research (IMSR), and Centre of Membrane Proteins and Receptors (COMPARE), University of Birmingham, Birmingham, UK.
[2]University of Lille, Institut National de la Santé et de la Recherche Médicale (INSERM), Centre Hospitalier Universitaire de Lille (CHU Lille), Institute Pasteur Lille, U1190 -European Genomic Institute for Diabetes (EGID), F59000, Lille, France.
[3]San Raffaele Diabetes Research Institute, IRCCS Ospedale San Raffaele, Milan, Italy.
[4]Vita-Salute San Raffaele University, Milan, Italy.
[5]Centre for Health, Ageing and Understanding Disease, Department of Biosciences, School of Science and Technology, Nottingham Trent University, Nottingham, UK.
[6]Oxford Centre for Diabetes, Endocrinology and Metabolism (OCDEM), NIHR Oxford Biomedical Research Centre, Churchill Hospital, Radcliffe Department of Medicine, University of Oxford, Oxford, UK.

*Correspondence should be addressed to:
d.hodson@ocdem.ox.ac.uk, c.ludwig@bham.ac.uk, d.tennant@bham.ac.uk

Key words: Glucose tracing, islet, metabolism, pyruvate, lactate, LDH, pyruvate dehydrogenase, GC-MS, NMR

bioRxiv preprint doi: https://doi.org/10.1101/2022.12.21.521364; this version posted December 21, 2022. The copyright holder for this preprint (which was not certified by peer review) is the author/funder, who has granted bioRxiv a license to display the preprint in perpetuity. It is made available under aCC-BY-NC 4.0 International license.

ABSTRACT

Using $^{13}C_6$ glucose labeling coupled to GC-MS and 2D ^{1}H-^{13}C HSQC NMR spectroscopy, we have obtained a comparative high-resolution map of glucose fate underpinning steady state insulin release and β cell function. In both mouse and human islets, the contribution of glucose to the TCA cycle is similar. Pyruvate-fueling of the TCA cycle is found to be mediated primarily by the activity of pyruvate dehydrogenase (PDH), with only a limited contribution from pyruvate carboxylase (PC). While conversion of pyruvate to lactate by lactate dehydrogenase (LDH) can be detected in both species, lactate accumulation via this route is six-fold higher in human islets. Transcriptomic analysis reveals that human β cells specifically express lactate dehydrogenase B (LDHB) at high levels, in keeping with the phenotype of patients harboring gain-of-function mutations in MCT1/ SLC16A1 (HHF7). Thus, glycolytically-derived acetyl CoA preferentially feeds the TCA cycle in both mouse and human β cells. However, human β cells possess the machinery needed to generate extra-mitochondrial lactate, which might reflect a key mechanism to balance the reducing activity of NADH-producing pathways.

bioRxiv preprint doi: https://doi.org/10.1101/2022.12.21.521364; this version posted December 21, 2022. The copyright holder for this preprint (which was not certified by peer review) is the author/funder, who has granted bioRxiv a license to display the preprint in perpetuity. It is made available under aCC-BY-NC 4.0 International license.

INTRODUCTION

β cells are highly-adapted as glucose sensors and need to balance glucose-dependent insulin release with housekeeping metabolic functions. The traditional view of β cell metabolism focuses on a tight relationship between blood glucose concentration, oxidative phosphorylation and stimulus-secretion coupling. Following a rise in glycemia, glucose enters the β cell through facilitated transport via low affinity glucose transporters (GLUT1 and GLUT2 in humans and rodents, respectively) (De Vos et al., 1995; Thorens et al., 1988). Glucose is then phosphorylated by a low affinity hexokinase, glucokinase (GK), leading to closure of the ATP-sensitive potassium (K_{ATP}) channels (reviewed in (Rorsman and Ashcroft, 2018; Rutter et al., 2015)). The increase in membrane voltage then drives Ca^{2+} flux through voltage-dependent Ca^{2+} channels (Rorsman and Ashcroft, 2018), which together with amplifying signals (amino acids, isocitrate, cAMP etc) (Ferdaoussi et al., 2015; Henquin, 2000; Rutter et al., 2015), drives first and second phase insulin granule exocytosis. Direct conversion of pyruvate to lactate is thought to be suppressed in the β cell due to low levels of lactate dehydrogenase A (*LDHA*) (Ainscow et al., 2000; Pullen et al., 2010; Schuit et al., 2012; Sekine et al., 1994), ensuring that the majority of pyruvate enters the TCA cycle.

Recent studies have challenged the canonical view of β cell metabolism by showing that ATP/ADP generation is highly compartmentalized, with the extra-mitochondrial phosphoenolpyruvate (PEP) cycle being a major trigger of K_{ATP} channel closure and insulin secretion (Foster et al., 2022; Lewandowski et al., 2020). Following membrane depolarization and Ca^{2+} influx, the rise in ADP activates oxidative phosphorylation (OxPhos) to sustain insulin secretion. These two complementary states are believed to dictate the mitochondrial fate of pyruvate. The electrically silent phase, which is characterized by a high ATP/ADP ratio, raises mitochondrial voltage to stall the TCA cycle, and activate anaplerotic flux through pyruvate carboxylase (PC) and the PEP cycle to support pyruvate kinase (PK) and initiate insulin secretion. Following membrane depolarization, the rise in ADP supports a highly oxidative state that depends on high TCA cycle flux and pyruvate consumption by pyruvate dehydrogenase (PDH), which supports OxPhos and sustained secretion (Foster et al., 2022; Lewandowski et al., 2020; Merrins et al., 2022).

Despite the clear importance of metabolism for β cell insulin release and phenotype, we are still lacking a high-resolution, integrated view of β cell glucose fate. In particular, most data using glucose tracing and GC-MS/NMR spectroscopy has been derived from insulinoma cell lines, which provide the requisite cell mass for metabolite detection/annotation. However, insulinoma cell lines have to balance the need for insulin secretion with proliferation, an energy-consuming process (Alves et al., 2015; Cline et al., 2004; Cline et al., 2011; Lu et al., 2002b; Malinowski et al., 2020; Simpson et al., 2006), and fail to display normal cell heterogeneity known to influence metabolism (Benninger and Hodson, 2018; Benninger and Kravets, 2021; Nasteska et al., 2021). In addition, species-differences in islet cell composition and β cell function have been described (Cabrera et al., 2006; Hodson et al., 2013; Rodriguez-Diaz et al., 2011), yet their influence on energetics is still unclear. Lastly, bulk metabolomics has been informative for understanding β cell metabolism (Spegel et al., 2013; Wallace et al., 2013) and, while sensitive, lacks the resolution required to pinpoint glucose fate during glycolysis and the TCA cycle. Thus, our understanding of β cell glucose metabolism remains incomplete.

bioRxiv preprint doi: https://doi.org/10.1101/2022.12.21.521364; this version posted December 21, 2022. The copyright holder for this preprint (which was not certified by peer review) is the author/funder, who has granted bioRxiv a license to display the preprint in perpetuity. It is made available under aCC-BY-NC 4.0 International license.

In the present study, we combine GC-MS-based $^{13}C_6$ glucose tracing with the resolution of 2D ^{1}H-^{13}C HSQC NMR multiplet analysis to map glucose fate in islets with high sensitivity. By applying this dual approach to human and mouse samples, we are able to provide a detailed cross-species depiction of glucose metabolism. By examining ^{13}C labelling patterns, we confirm that PDH is the major contributor to the TCA cycle. We further show that pyruvate is directly converted to lactate in both human and mouse islets. However, lactate accumulation is much higher in human islets, which specifically express *LDHB* in the β cell compartment. We thus provide a detailed view of mouse and human islet metabolism, show that human β cells generate significant lactate levels, and suggest that the role of lactate in β cell metabolism should be revisited.

bioRxiv preprint doi: https://doi.org/10.1101/2022.12.21.521364; this version posted December 21, 2022. The copyright holder for this preprint (which was not certified by peer review) is the author/funder, who has granted bioRxiv a license to display the preprint in perpetuity. It is made available under aCC-BY-NC 4.0 International license.

RESULTS

Glucose contribution to TCA cycle in human and mouse islets

To investigate glucose handling, mouse and human islets were incubated overnight with $^{13}C_6$ glucose prior to metabolite extraction and GC-MS and 2D $^{1}H,^{13}C$ HSQC-NMR spectroscopy (**Figure 1A**). To allow sufficient glucose flux for detection of ^{13}C incorporation into TCA metabolites, without inducing glucotoxicity, 10 mM $^{13}C_6$ glucose was used. The incorporation of ^{13}C from $^{13}C_6$ glucose into the TCA cycle metabolites was then established via mass isotopologues distribution (MID) analysis **(Figure 1B)**.

Suggesting a similar progression of glycolysis and the TCA cycle, glucose incorporation into the major metabolites malate, alanine and glutamate was not different between mouse and human islets **(Figure 1C-E)**. However, a slight but significant increase in m+2/m+3 aspartate and fumarate was detected in mouse versus human islets (**Figure 1F and G**), reflecting an increased contribution of glucose-derived pyruvate into the TCA cycle via acetyl CoA. Total aspartate and alanine levels did not differ between the species (**Figure 1H and I**), whereas malate and fumarate levels (**Figure 1J and K**) were decreased in mouse. Glutamate levels were ~3-fold higher in mouse versus human islets, despite similar MIDs, implying that there is a larger contribution of non-labelled glutamate to the total glutamate pool in this species e.g. through glutamine transport (**Figure 1L**).

Pyruvate management in human and mouse islets

To obtain a higher definition view of pyruvate management, its contribution to the production of alanine and lactate was assessed. In both species, glucose incorporation could be detected in m+2 and m+3 lactate, likely derived from the TCA cycle and direct pyruvate conversion, respectively (**Figure 2A-C**). While the MID for alanine was similar in islets from both species (**Figure 1E**), the accumulation of m+ 2 and m+3 lactate was significantly (~ 6-fold) higher in humans (**Figure 2A**). In line with the larger size of human islets, or the increased proportion of α cells, the total amount of lactate was higher in human than in mouse islets (**Figure 2B-D**).

While accumulation of m+2 lactate was expected, we were surprised to detect significant m+3 lactate accumulation in human islets, since *Ldha* has been shown to be "disallowed" in mouse β cells, hence preventing alternative fates for pyruvate (Ainscow et al., 2000; Pullen et al., 2010; Schuit et al., 2012; Sekine et al., 1994). However, recent studies in cancer cells have shown that pyruvate to lactate conversion is unaffected in single knockouts of LDHA and LDHB, and only in a double LDHA/B knockout is pyruvate no longer converted to lactate (Deng et al., 2022; Ždralević et al., 2018). Thus, LHDB can compensate for LDHA activity. Moreover, glucose-stimulated lactate production and oscillations were detected in intact mouse islets using a biosensor approach (Sdao et al., 2021). In accordance, we find that β cells predominantly and specifically express *LDHB* (**Figure 2E**). Moreover, we could not exclude the possibility that LDHA may also catalyze pyruvate to lactate conversion in β cells as they contain LDHA mRNA, albeit at low quantities, based on both single cell RNA-sequencing and bulk RNA-sequencing of FACS sorted α cells and β cells (**Figure 2E and F**). This is consistent with the open chromatin conformation and transcription factor binding to this promoter in the human islet (**Figure 2G**).

High resolution annotation of $^{13}C_6$ glucose tracing data

bioRxiv preprint doi: https://doi.org/10.1101/2022.12.21.521364; this version posted December 21, 2022. The copyright holder for this preprint (which was not certified by peer review) is the author/funder, who has granted bioRxiv a license to display the preprint in perpetuity. It is made available under aCC-BY-NC 4.0 International license.

To identify isotopomer patterns with high-resolution, the MID analysis of $^{13}C_6$ glucose-traced human and mouse islets was annotated with 2D ^{1}H-^{13}C HSQC NMR multiplet analysis. From uniformly labeled glucose, ^{13}C atoms are incorporated into the metabolites of the TCA cycle through the activity of PDH and PC (**Figure 3A, B**). This leads to the formation of labeling patterns within the chemical structure of each metabolite that are specific to the pathway from which they are produced (**Figure 3A, B**). Therefore, the positions of ^{13}C atoms within each metabolite can be utilized to elucidate the relative activities of PDH and PC. To define the different isotopomer patterns a numerical notation was used, where the numbers 0 and 1 indicate ^{12}C and ^{13}C atoms, respectively. Confirming the accuracy of the approach, the accumulation of lactate$_{111}$ (i.e. fully-labeled lactate) was significantly higher in human compared to mouse islets, in line with the MID glucose-tracing data (**Figure 2A-C**) (**Figure 3C-E**).

TCA cycle depends more on PDH than PC flux in human and mouse islets

In both human and mouse islets, lactate$_{110}$ made a greater contribution to the m+2 isotopologue pool than the other possible isotopomers (**Figure 3C-E**). This finding suggests that lactate is produced from the oxidative TCA cycle rather than the reductive metabolism of PC-derived glutamate, from which pyruvate$_{011}$ and then lactate$_{011}$ would arise (**Figure 3C-E**). We also noticed that the majority of alanine was either 000 or 111, with only a very minor contribution to the other isotopomers (**Figure 3F-H**). As such, the labeled portion of alanine is produced from pyruvate upstream of the TCA cycle, meaning that the accumulation of pyruvate$_{110}$ from malate$_{1100}$ is mostly employed to regenerate lactate$_{110}$ (**Figure 3F-H**). Alanine$_{111}$ accumulation was slightly (~20%) higher in human than mouse islets, reflecting a greater contribution of transamination toward amino acid production (**Figure 3F-H**). Supporting the lactate isotopomer data, the contribution of $^{13}C_6$ glucose to the labeling patterns of glutamate was found to be similar in humans and mice (**Figure 3I, J**). In both species, the most abundant labeled isotopomer was glutamate$_{00011}$ (**Figure 3I, J**), which is derived from TCA cycle flux through the activity of PDH (**Figure 3A, J**).

Together, these findings provide further evidence that pyruvate management in the pancreatic β cell occurs primarily through PDH at the stimulatory glucose concentration used here (Alves et al., 2015; Lu et al., 2002a).

bioRxiv preprint doi: https://doi.org/10.1101/2022.12.21.521364; this version posted December 21, 2022. The copyright holder for this preprint (which was not certified by peer review) is the author/funder, who has granted bioRxiv a license to display the preprint in perpetuity. It is made available under aCC-BY-NC 4.0 International license.

DISCUSSION

Using $^{13}C_6$ glucose labeling coupled to GC-MS and 2D ^{1}H-^{13}C HSQC NMR spectroscopy, we have been able toobtain a high-resolution map of glucose fate within human and mouse islets. Unexpectedly, both human and mouse islets accumulate m+2 and m+3 lactate, meaning that lactate produced downstream of the TCA cycle (m+2) as well as via pyruvate -> lactate conversion (m+3) contribute equally to overall lactate production. However, pyruvate -> lactate conversion was much higher (~ 6-fold) in human compared to mouse islets, most likely due to the actions of LDHB. Finally, we show that labeled lactate and glutamate accumulate as $lactate_{110}$ and $glutamate_{00011}$, confirming greater flux through PDH versus PC in both species. The major findings are schematically represented in **Figure 4**.

The observation that the islet lactate pool is derived from both TCA cycle- and pyruvate-derived sources suggests that mechanisms must be in place for direct pyruvate conversion, particularly in the human islet. In many tissues, pyruvate would be converted to lactate by LDH, however, the major *Ldha* subunit of the enzyme has been shown to be expressed at very low levels, disallowed or absent in the murine pancreatic β cell (Lemaire et al., 2016; Pullen et al., 2010; Sekine et al., 1994). Analysis of multiple published scRNA-seq datasets showed that *LDHA* is expressed in the human pancreatic β cell, albeit at much lower levels than in neighboring α cells. It should be noted that the levels detected could represent contamination artefacts. In the presence of other LDH isoforms (*vide infra*), these relatively low levels of LDHA are likely sufficient to catalyze lactate production given the abundance of its substrate pyruvate in the β cell. Human β cells were also found to specifically and strongly express *LDHB*, which encodes the beta subunit of LDH. While an increased ratio of LDHB:LDHA is thought to catalyze production of pyruvate from lactate (Nam et al., 2016), recent studies have shown that LDHB-alone can replace the activity of LDHA to produce lactate. Indeed, deletion of both *LDHA* and *LDHB* is required to reduce lactate secretion in cells, whereas deletion of either LDHA or LDHB is without effect (Deng et al., 2022; Ždralević et al., 2018).

Providing strong human genetic evidence for our findings here, studies have shown that Hyperinsulinemic hypoglycemic familial 7 (HHF7) patients develop exercise-induced hyperinsulinemia due to gain-of-function mutations in the cell surface lactate transporter MCT1/SLC16A1 (Otonkoski et al., 2007; Pullen et al., 2012). During exercise, when extracellular lactate levels are increased, cytoplasmic pyruvate accumulation is able to fuel the TCA cycle, leading to non glucose-dependent insulin release (Otonkoski et al., 2007; Pullen et al., 2012). To allow such lactate -> pyruvate conversion, human β cells must express sufficient LDH, and in particular *LDHB*, as shown here

It is also possible that other cell types within the islets, such as α-cells, contribute to the accumulation of lactate. In particular, human α cells account for ~35% of the entire islet and express *LDHA* at levels six times higher than β cells (Moin et al., 2020; Sanchez et al., 2021). However, a major source of α cell lactate is via monocarboxylate transporters (Pullen and Rutter, 2013; Schuit et al., 2012; Zaborska et al., 2020), which are unlikely to play a role here as lactate was absent from the tracing medium. In addition, while the total amount of lactate was only doubled in humans compared to mice, the m+3 lactate accumulation was ~six-fold higher in human *versus* mouse islets. Taken together these data suggest that, although there might be a contribution of lactate from α cells, this is unlikely to account for the whole m+3 lactate increase detected here.

bioRxiv preprint doi: https://doi.org/10.1101/2022.12.21.521364; this version posted December 21, 2022. The copyright holder for this preprint (which was not certified by peer review) is the author/funder, who has granted bioRxiv a license to display the preprint in perpetuity. It is made available under aCC-BY-NC 4.0 International license.

Human and mouse islets display a greater accumulation of lactate$_{110}$, rather than lactate$_{011}$. While the accumulation of lactate$_{110}$ is indistinguishable in the PDH- and PC-mediated TCA cycle, the 011 isotopomer would only derive from the reductive metabolism of PC-derived glutamate. Corroborating this, in islets from both species, the major glutamate isotopomer derived from exogenous $^{13}C_6$ glucose was glutamate$_{00011}$. Although glutamate is not a TCA cycle metabolite, it is in rapid exchange with α-KG and can be used as a read-out of TCA cycle flux through PDH or PC. Consequently, the accumulation of glutamate$_{00011}$ provides further evidence for a higher reliance of the TCA cycle on the activity of PDH, rather than PC. Although PC and PDH were thought to contribute equally to the TCA cycle in β-cells (Cline et al., 2004; Cline et al., 2011; Simpson et al., 2006), previous studies have shown that high glucose concentrations in vitro, more reflective of those seen post-prandially in vivo, are associated with an increase toward PDH activity (Alves et al., 2015; Lewandowski et al., 2020; Lu et al., 2002a). Our studies thus show that the relative contribution of PC to the TCA cycle is much lower than PDH (~20%), confirming findings from Alves et al in glucose-traced INS-1 cells (Alves et al., 2015) and Lewandowski et al in human islets (Lewandowski et al., 2020). While anaplerosis through PC is relatively limited in the rβ cell, we note that glucose carbons can repeatedly transit the PEP cycle to generate ATP/ADP independently of oxidative phosphorylation (Lewandowski et al., 2020). As such, PC is able to make disproportionate contributions to K_{ATP} channel closure, and hence the triggering phase of insulin secretion, by generating localized increases in ATP/ADP (Merrins et al., 2022). However, insulin secretion is not the only energy sink on the β cell, and glucose flux through PDH is likely to provide a source of glucose oxidation to support other demands such as continued insulin release and protein synthesis.

What might be the role of direct pyruvate to lactate conversion in pancreatic β cells? Since the action of LDH leads to oxidation of NADH to NAD^+, lactate accumulation could provide a source of reducing equivalents to support other NADH-producing metabolic pathways. Providing evidence for a contribution of pyruvate to lactate conversion in NADH/NAD^+ balance, the alanine isotopomer distribution showed almost exclusively the accumulation of alanine$_{000}$ and alanine$_{111}$. This finding suggests that the pyruvate accumulated downstream of the TCA cycle is mostly employed in the production of lactate$_{110}$. Since the conversion of pyruvate to lactate is associated with the generation of cytosolic NAD^+, higher levels of lactate$_{111}$ in humans might reflect an increase in the activity of NADH-producing pathways relative to rodents. However, β cells are thought to already have a large capacity to produce reducing equivalents, for example via the glycerol phosphate and malate-aspartate shuttles (Campbell and Newgard, 2021). Moreover, while LDH was found to form nanodomains with K_{ATP} channels, supporting production of high local levels of NAD+, levels of lactate were insufficient to influence K_{ATP} channel conductance (Ho et al., 2022). Lactate might be relatively more important when REDOX capacity is stretched, for example during ageing and ER stress, when NADH/NAD^+ pathways become more pronounced (Covarrubias et al., 2020). As such, future studies are warranted to investigate the functional impact of pyruvate to lactate conversion on β cell metabolism and function.

There are a number of limitations in the present studies. Firstly, $^{13}C_6$ glucose labeling was conducted in whole islets rather than purified cell populations, excluding definitive annotation of β cell metabolism. However, since ^{13}C becomes diluted following achievement of steady-state, a large number (hundreds) of islets are required for accurate signal detection, particularly so for NMR. Secondly, the results are derived from male and female non-diabetic

bioRxiv preprint doi: https://doi.org/10.1101/2022.12.21.521364; this version posted December 21, 2022. The copyright holder for this preprint (which was not certified by peer review) is the author/funder, who has granted bioRxiv a license to display the preprint in perpetuity. It is made available under aCC-BY-NC 4.0 International license.

donors, as well as male mouse islets. Going forwards, results should be stratified according to age, sex, BMI and T2D status, although we note that 800 MHz NMR capacity, probe time and helium availability largely preclude such experiments for the moment. Thirdly, whereas isotopologue and isotopomer data accurately delineate glucose fluxes and pyruvate management in islets, they are unable to measure the relative contribution of the identified pathways to insulin secretion. Nonetheless, our data provide a detailed and interrogable map of glucose metabolism pertaining to steady state insulin release in human and mouse islets, as well as other critical β cell housekeeping functions. Lastly, glucotoxicity might induce the upregulation of disallowed genes in β-cells (Bensellam et al., 2018). However, it is unlikely that the timings (12 hrs) and glucose concentration (10 mM) used here would overtly influence human β-cell lactate production, since *LDHA* or *LDHB* were not found to be differentially expressed in human islets exposed to 22.2 mM glucose for 4 days (Marselli et al., 2020).

In summary, by combining MID and multiplet analyses, we show that glucose makes a similar contribution to glycolysis and the TCA cycle in human and mouse islets. Furthermore, the isotopomer distribution confirms that, in both species, the relative activity of PDH is much higher than that of PC at elevated glucose concentration. However, the production of fully-labeled lactate was found to be significantly higher in human versus mouse islets, which is likely due to high expression levels of *LDHB*. Together, these results demonstrate that lactate production needs to be reconsidered in light of human beta cell metabolism and REDOX balance.

bioRxiv preprint doi: https://doi.org/10.1101/2022.12.21.521364; this version posted December 21, 2022. The copyright holder for this preprint (which was not certified by peer review) is the author/funder, who has granted bioRxiv a license to display the preprint in perpetuity. It is made available under aCC-BY-NC 4.0 International license.

METHODS

Ethics

Animal studies were regulated by the Animals (Scientific Procedures) Act 1986 of the U.K. (Personal Project Licences P2ABC3A83 and PP1778740). Approval was granted by the University of Birmingham's Animal Welfare and Ethical Review Body (AWERB).

Human islets (Lille): human pancreatic tissues were harvested from brain-dead adult donors in accordance with the Lille clinical islet transplantation program's traceability requirements (clinicaltrials.gov, NCT01123187, NCT00446264, NCT01148680), and were approved in agreement with French regulations and the Ethical Committees of the University of Lille and the Centre Hospitalier Régional Universitaire de Lille.

Human islets (Milan): the use of human islets for research was approved by the Ethics Committee of San Raffaele Hospital in Milan (IPF002-2014).

Studies with human tissue were approved by the University of Birmingham Ethics Committee, the University of Oxford Ethics Committee, as well as the National Research Ethics Committee (REC reference 16/NE/0107, Newcastle and North Tyneside, UK).

Mouse islets

Male 8 to 12 week-old CD1 mice (Charles River stock no. 022) were used as tissue donors. Briefly, animals were culled using a schedule-1 method followed by injection of the common bile duct with 1 mg/mL collagenase NB 8 (Serva) in RPMI 1640 (Gibco) and pancreas dissection. After dissection, the pancreas was incubated in a water bath at 37°C for 12 min. Subsequently, the tissues were shaken in 15 mL of RPMI 1640 and centrifuged for 1 min at 1500 rpm three times to induce mechanical digestion. Islets were separated using Histopaque-1119 and 1083 (Sigma-Aldrich) gradients, before hand-picking and culture. Unless otherwise stated, the islets obtained were kept in culture in RPMI 1640 supplemented with 10% fetal bovine serum (FBS, Gibco), 100 units/mL penicillin, and 100 µg/mL streptomycin (Sigma-Aldrich), at 37°C and 5% CO_2.

Human islets

Islets were provided by the San Raffaele Diabetes Research Institute (DRI), Milan, Italy (ECIT Islet for Basic Research program), as well as the Translational Research for Diabetes at the University of Lille, Lille, France.

Upon receipt, the islets were cleared of possible debris via filtration with a 40 µm cut-off filter, hand-picked and cultured in CMRL medium (Corning) supplemented with 5.5 mM glucose (Sigma-Aldrich), 10% FBS, 100 units/mL penicillin, 100 µg/mL streptomycin and 0.1% amphotericin B (Sigma-Aldrich) at 37°C and 5% CO_2. Donor characteristics are reported in Table 1.

$^{13}C_6$ glucose tracing

For $^{13}C_6$ glucose tracing, 60 (for GC-MS) or 150-230 (for NMR) islets were used. Isolated islets were cultured in RPMI 1640, no glucose medium (Gibco), supplemented with 10% BSA, 10% FBS, 100 units/mL penicillin, and 100 µg/mL streptomycin plus 10 mM $^{13}C_6$ glucose (Sigma-

bioRxiv preprint doi: https://doi.org/10.1101/2022.12.21.521364; this version posted December 21, 2022. The copyright holder for this preprint (which was not certified by peer review) is the author/funder, who has granted bioRxiv a license to display the preprint in perpetuity. It is made available under aCC-BY-NC 4.0 International license.

Aldrich). After 24 h, the metabolites were extracted adding HPLC-grade methanol, HPLC-grade distilled H_2O containing 1 µg/mL D6-glutaric acid and HPLC-grade chloroform (all from Sigma-Aldrich) in a 1:1:1 ratio, to the islets. Following centrifugation, the polar fractions were collected and vacuum dried before either GC-MS or NMR analyses.

GC-MS

The dried polar extracts were prepared for GC-MS analysis through solubilization in 40 µL of 2% methoxyamine hydrochloric acid in pyridine (Fisher Scientific) at 60°C for 60 min and derivatization with 60 µL of N-tertbutyldimethylsilyl-N-methyltrifluoroacetamide (MTBSTFA) with 1% tertbutyldimethyl-chlorosilane (TBDMCS) (both from Sigma-Aldrich). The suspension was further incubated at 60°C for 60 min, before being centrifuged at 13300 rpm for 10 min at 4°C and transferred to chromatography vials with a glass insert (Restek) for GC-MS analysis. The samples were analyzed on an Agilent 8890 GC and 5977B MSD system. To do this, 1 µL of sample was injected in splitless mode with helium carrier gas at a rate of 1.0 mL/min. The compound detection was carried out in scan mode and total ion counts of each metabolite were normalized to the internal standard D6-glutaric acid using an in-house MATLAB script.

NMR spectroscopy

Following the $^{13}C_6$ glucose tracing, the dried polar metabolites were resuspended in 60 µL of phosphate buffer: 57.8 mM disodium phosphate (Na_2HPO_4, Sigma-Aldrich), 42.2 mM monosodium phosphate (NaH_2PO_4, Sigma-Aldrich), 0.5 mM 3-(trimethylsilyl) propionic-2,2,3,3-d4 acid sodium salt (D4-TMSP, Sigma-Aldrich) in deuterium oxide (D_2O, Sigma-Aldrich). Subsequently, the samples were centrifuged for 10 min at 14800 rpm and sonicated in an ultrasonic bath for 5 min, before being loaded into NMR tubes (outer diameter: 1.7 mm, Bruker) for acquisition. A Bruker Neo 800 MHz NMR spectrometer equipped with a 1.7 mm z-PFG TCI Cryoprobe was used to acquire 2D $^{1}H,^{13}C$-HSQC NMR spectra. The HSQC spectra were acquired with echo/anti-echo gradient coherence selection with an additional pre-saturation for suppressing the residual water resonance. The spectral widths were 15.6298 ppm and 189.7832 ppm in the ^{1}H and ^{13}C dimension, 512 complex data points were acquired for the ^{1}H dimension and 25% (512) out of 2048 complex data points were acquired for the ^{13}C indirect dimension using a non-uniform sampling scheme. Apparent $^{13}C,^{13}C$ J-coupling was enhanced four-fold. The interscan relaxation delay was set to 1.5 s. 2D $^{1}H,^{13}C$-HSQC spectra were reconstructed via the compressed sensing IRLS algorithm using the MDDNMR (version 2.5) (Kazimierczuk and Orekhov, 2011) and NMRPipe (version 9.2) (Delaglio et al., 1995) software. All NMR spectra were analysed in the MATLAB based MetaboLab software package (Ludwig and Günther, 2011).

Transcriptomics analysis

Quantification data for all published scRNA-seq datasets were kindly provided by Leon Van Gurp (van Gurp et al., 2022). In brief, pseudo-counts were normalized for each data set using Seurat (Satija et al., 2015), and the cell identity was assigned based on the requirement for hormone gene expression to be in the top 1% expressed genes in each cell using Aucell (Aibar et al., 2017). Quantification for published FACS sorted alpha and β cells were obtained from GEO database repository under Arda et al (Arda et al., 2016). The raw read files for each cell type were merged, trimmed and the transcripts were quantified using Kallisto (Bray et al.,

bioRxiv preprint doi: https://doi.org/10.1101/2022.12.21.521364; this version posted December 21, 2022. The copyright holder for this preprint (which was not certified by peer review) is the author/funder, who has granted bioRxiv a license to display the preprint in perpetuity. It is made available under aCC-BY-NC 4.0 International license.

2016) or aligned and quantified as previously described (Akerman et al., 2020), with similar results.

Statistics and reproducibility

Statistical significance was assessed with GraphPad Prism 9 (version 9.2.0). Pairwise comparisons were made using Welch's test (assuming non-equal standard deviation between groups). Multiple interactions were determined using one-way ANOVA or two-way ANOVA, with Sidak's post-hoc test.

All error bars represent mean ± S.E.M. and a p-value less than 0.05 was considered significant: *p< 0.05; **p< 0.01; ***p< 0.001, ****p<0.0001.

bioRxiv preprint doi: https://doi.org/10.1101/2022.12.21.521364; this version posted December 21, 2022. The copyright holder for this preprint (which was not certified by peer review) is the author/funder, who has granted bioRxiv a license to display the preprint in perpetuity. It is made available under aCC-BY-NC 4.0 International license.

AUTHOR CONTRIBUTIONS

F.C. performed experiments, analysed data and wrote the manuscript. D.N. and H.R.M. performed experiments. Z.J. and I.A. performed bioinformatic analysis. R.N., L.P., C.B., F.P. and J.K-C. isolated and provided human islets. C.L. performed $^{1}H,^{13}C$-HSQC NMR experiments and analysis. G.G.L., D.T. and J.R. ran GC-MS on $^{13}C_6$ glucose labelled samples and provided analysis. D.J.H. supervised the studies, provided analysis and wrote the manuscript with contributions from C.L. and D.T. All authors read and approved the studies.

ACKNOWLEDGEMENTS

D.J.H. was supported by MRC (MR/N00275X/1 and MR/S025618/1) and Diabetes UK (17/0005681) Project Grants, as well as a UKRI ERC Frontier Research Guarantee Grant (EP/X026833/1). This project has received funding from the European Research Council (ERC) under the European Union's Horizon 2020 research and innovation programme (Starting Grant 715884 to D.J.H.). G.G.L. was supported by a Wellcome Trust Senior Fellowship (104612/Z/14/Z). D.T. was supported by a Cancer Research UK Programme Grant (C42109/A24747). The research was funded by the National Institute for Health Research (NIHR) Oxford Biomedical Research Centre (BRC). The views expressed are those of the author(s) and not necessarily those of the NHS, the NIHR or the Department of Health. We would like to acknowledge the support and resources of the Birmingham Metabolic Tracer Analysis Core. We thank Dr. Matthew J. Merrins (University of Wisconsin) for critical comments on the manuscript.

DISCLOSURE STATEMENT

D.J.H. receives licensing revenue from Celtarys Research.

bioRxiv preprint doi: https://doi.org/10.1101/2022.12.21.521364; this version posted December 21, 2022. The copyright holder for this preprint (which was not certified by peer review) is the author/funder, who has granted bioRxiv a license to display the preprint in perpetuity. It is made available under aCC-BY-NC 4.0 International license.

REFERENCES

Aibar, S., Gonzalez-Blas, C.B., Moerman, T., Huynh-Thu, V.A., Imrichova, H., Hulselmans, G., Rambow, F., Marine, J.C., Geurts, P., Aerts, J., et al. (2017). SCENIC: single-cell regulatory network inference and clustering. Nat Methods *14*, 1083-1086.

Ainscow, E.K., Zhao, C., and Rutter, G.A. (2000). Acute overexpression of lactate dehydrogenase-A perturbs beta-cell mitochondrial metabolism and insulin secretion. Diabetes *49*, 1149-1155.

Akerman, I., Kasaai, B., Bazarova, A., Sang, P.B., Peiffer, I., Artufel, M., Derelle, R., Smith, G., Rodriguez-Martinez, M., Romano, M., et al. (2020). A predictable conserved DNA base composition signature defines human core DNA replication origins. Nat Commun *11*, 4826.

Akerman, I., Tu, Z., Beucher, A., Rolando, D.M.Y., Sauty-Colace, C., Benazra, M., Nakic, N., Yang, J., Wang, H., Pasquali, L., et al. (2017). Human Pancreatic beta Cell lncRNAs Control Cell-Specific Regulatory Networks. Cell Metab *25*, 400-411.

Alves, T.C., Pongratz, R.L., Zhao, X., Yarborough, O., Sereda, S., Shirihai, O., Cline, G.W., Mason, G., and Kibbey, R.G. (2015). Integrated, Step-Wise, Mass-Isotopomeric Flux Analysis of the TCA Cycle. Cell Metab *22*, 936-947.

Arda, H.E., Li, L., Tsai, J., Torre, E.A., Rosli, Y., Peiris, H., Spitale, R.C., Dai, C., Gu, X., Qu, K., et al. (2016). Age-Dependent Pancreatic Gene Regulation Reveals Mechanisms Governing Human beta Cell Function. Cell Metab *23*, 909-920.

Benninger, R.K.P., and Hodson, D.J. (2018). New Understanding of β-Cell Heterogeneity and In Situ Islet Function. Diabetes *67*, 537-547.

Benninger, R.K.P., and Kravets, V. (2021). The physiological role of β-cell heterogeneity in pancreatic islet function. Nature Reviews Endocrinology.

Bensellam, M., Jonas, J.C., and Laybutt, D.R. (2018). Mechanisms of beta-cell dedifferentiation in diabetes: recent findings and future research directions. J Endocrinol *236*, R109-R143.

Bray, N.L., Pimentel, H., Melsted, P., and Pachter, L. (2016). Near-optimal probabilistic RNA-seq quantification. Nat Biotechnol *34*, 525-527.

Cabrera, O., Berman, D.M., Kenyon, N.S., Ricordi, C., Berggren, P.O., and Caicedo, A. (2006). The unique cytoarchitecture of human pancreatic islets has implications for islet cell function. Proceedings of the National Academy of Sciences of the United States of America *103*, 2334-2339.

Campbell, J.E., and Newgard, C.B. (2021). Mechanisms controlling pancreatic islet cell function in insulin secretion. Nat Rev Mol Cell Biol *22*, 142-158.

Cline, G.W., Lepine, R.L., Papas, K.K., Kibbey, R.G., and Shulman, G.I. (2004). 13C NMR isotopomer analysis of anaplerotic pathways in INS-1 cells. J Biol Chem *279*, 44370-44375.

Cline, G.W., Pongratz, R.L., Zhao, X., and Papas, K.K. (2011). Rates of insulin secretion in INS-1 cells are enhanced by coupling to anaplerosis and Kreb's cycle flux independent of ATP synthesis. Biochem Biophys Res Commun *415*, 30-35.

Covarrubias, A.J., Perrone, R., Grozio, A., and Verdin, E. (2020). NAD+ metabolism and its roles in cellular processes during ageing. Nature Reviews Molecular Cell Biology *22*, 119-141.

De Vos, A., Heimberg, H., Quartier, E., Huypens, P., Bouwens, L., Pipeleers, D., and Schuit, F. (1995). Human and rat beta cells differ in glucose transporter but not in glucokinase gene expression. Journal of Clinical Investigation *96*, 2489-2495.

Delaglio, F., Grzesiek, S., Vuister, G., Zhu, G., Pfeifer, J., and Bax, A. (1995). NMRPipe: A multidimensional spectral processing system based on UNIX pipes. Journal of Biomolecular NMR *6*.

Deng, H., Gao, Y., Trappetti, V., Hertig, D., Karatkevich, D., Losmanova, T., Urzi, C., Ge, H., Geest, G.A., Bruggmann, R., et al. (2022). Targeting lactate dehydrogenase B-dependent mitochondrial metabolism affects tumor initiating cells and inhibits tumorigenesis of non-small cell lung cancer by inducing mtDNA damage. Cellular and Molecular Life Sciences *79*.

Enge, M., Arda, H.E., Mignardi, M., Beausang, J., Bottino, R., Kim, S.K., and Quake, S.R. (2017). Single-Cell Analysis of Human Pancreas Reveals Transcriptional Signatures of Aging and Somatic Mutation Patterns. Cell *171*, 321-330 e314.

bioRxiv preprint doi: https://doi.org/10.1101/2022.12.21.521364; this version posted December 21, 2022. The copyright holder for this preprint (which was not certified by peer review) is the author/funder, who has granted bioRxiv a license to display the preprint in perpetuity. It is made available under aCC-BY-NC 4.0 International license.

Ferdaoussi, M., Dai, X., Jensen, M.V., Wang, R., Peterson, B.S., Huang, C., Ilkayeva, O., Smith, N., Miller, N., Hajmrle, C., et al. (2015). Isocitrate-to-SENP1 signaling amplifies insulin secretion and rescues dysfunctional beta cells. J Clin Invest *125*, 3847-3860.

Foster, H.R., Ho, T., Potapenko, E., Sdao, S.M., Huang, S.M., Lewandowski, S.L., VanDeusen, H.R., Davidson, S.M., Cardone, R.L., Prentki, M., et al. (2022). β-cell deletion of the PKm1 and PKm2 isoforms of pyruvate kinase in mice reveals their essential role as nutrient sensors for the KATP channel. eLife *11*.

Henquin, J.C. (2000). Triggering and amplifying pathways of regulation of insulin secretion by glucose. Diabetes *49*, 1751-1760.

Ho, T., Potapenko, E., Davis, D.B., and Merrins, M.J. (2022). A plasma membrane-associated glycolytic metabolon is functionally coupled to KATP channels in pancreatic α and β cells from humans and mice. bioRxiv.

Hodson, D.J., Mitchell, R.K., Bellomo, E.A., Sun, G., Vinet, L., Meda, P., Li, D., Li, W.H., Bugliani, M., Marchetti, P., et al. (2013). Lipotoxicity disrupts incretin-regulated human beta cell connectivity. Journal of Clinical Investigation *123*, 4182-4194.

Kazimierczuk, K., and Orekhov, V.Y. (2011). Accelerated NMR Spectroscopy by Using Compressed Sensing. Angewandte Chemie International Edition *50*, 5556-5559.

Lawlor, N., George, J., Bolisetty, M., Kursawe, R., Sun, L., Sivakamasundari, V., Kycia, I., Robson, P., and Stitzel, M.L. (2017). Single-cell transcriptomes identify human islet cell signatures and reveal cell-type–specific expression changes in type 2 diabetes. Genome Research *27*, 208-222.

Lemaire, K., Thorrez, L., and Schuit, F. (2016). Disallowed and Allowed Gene Expression: Two Faces of Mature Islet Beta Cells. Annu Rev Nutr *36*, 45-71.

Lewandowski, S.L., Cardone, R.L., Foster, H.R., Ho, T., Potapenko, E., Poudel, C., VanDeusen, H.R., Sdao, S.M., Alves, T.C., Zhao, X., et al. (2020). Pyruvate Kinase Controls Signal Strength in the Insulin Secretory Pathway. Cell Metabolism *32*, 736-750.e735.

Lu, Mulder, H., Zhao, P., Burgess, S.C., Jensen, M.V., Kamzolova, S., Newgard, C.B., and Sherry, A.D. (2002a). 13C NMR isotopomer analysis reveals a connection between pyruvate cycling and glucose-stimulated insulin secretion (GSIS). Proc Natl Acad Sci U S A *99*, 2708-2713.

Lu, D., Mulder, H., Zhao, P., Burgess, S.C., Jensen, M.V., Kamzolova, S., Newgard, C.B., and Sherry, A.D. (2002b). 13C NMR isotopomer analysis reveals a connection between pyruvate cycling and glucose-stimulated insulin secretion (GSIS). Proc Natl Acad Sci U S A *99*, 2708-2713.

Ludwig, C., and Günther, U.L. (2011). MetaboLab - advanced NMR data processing and analysis for metabolomics. BMC Bioinformatics *12*.

Malinowski, R.M., Ghiasi, S.M., Mandrup-Poulsen, T., Meier, S., Lerche, M.H., Ardenkjær-Larsen, J.H., and Jensen, P.R. (2020). Pancreatic β-cells respond to fuel pressure with an early metabolic switch. Scientific Reports *10*.

Marselli, L., Piron, A., Suleiman, M., Colli, M.L., Yi, X., Khamis, A., Carrat, G.R., Rutter, G.A., Bugliani, M., Giusti, L., et al. (2020). Persistent or Transient Human β Cell Dysfunction Induced by Metabolic Stress: Specific Signatures and Shared Gene Expression with Type 2 Diabetes. Cell Reports *33*.

Merrins, M.J., Corkey, B.E., Kibbey, R.G., and Prentki, M. (2022). Metabolic cycles and signals for insulin secretion. Cell Metabolism *34*, 947-968.

Moin, A.S.M., Cory, M., Gurlo, T., Saisho, Y., Rizza, R.A., Butler, P.C., and Butler, A.E. (2020). Pancreatic alpha-cell mass across adult human lifespan. Eur J Endocrinol *182*, 219-231.

Nam, K., Oh, S., and Shin, I. (2016). Ablation of CD44 induces glycolysis-to-oxidative phosphorylation transition via modulation of the c-Src-Akt-LKB1-AMPKalpha pathway. Biochem J *473*, 3013-3030.

Nasteska, D., Fine, N.H.F., Ashford, F.B., Cuozzo, F., Viloria, K., Smith, G., Dahir, A., Dawson, P.W.J., Lai, Y.-C., Bastidas-Ponce, A., et al. (2021). PDX1LOW MAFALOW β-cells contribute to islet function and insulin release. Nature Communications *12*, 674.

Otonkoski, T., Jiao, H., Kaminen-Ahola, N., Tapia-Paez, I., Ullah, M.S., Parton, L.E., Schuit, F., Quintens, R., Sipila, I., Mayatepek, E., et al. (2007). Physical exercise-induced

bioRxiv preprint doi: https://doi.org/10.1101/2022.12.21.521364; this version posted December 21, 2022. The copyright holder for this preprint (which was not certified by peer review) is the author/funder, who has granted bioRxiv a license to display the preprint in perpetuity. It is made available under aCC-BY-NC 4.0 International license.

hypoglycemia caused by failed silencing of monocarboxylate transporter 1 in pancreatic beta cells. American Journal of Human Genetics *81*, 467-474.

Pullen, T.J., Khan, A.M., Barton, G., Butcher, S.A., Sun, G., and Rutter, G.A. (2010). Identification of genes selectively disallowed in the pancreatic islet. Islets *2*, 89-95.

Pullen, T.J., and Rutter, G.A. (2013). When less is more: the forbidden fruits of gene repression in the adult beta-cell. Diabetes Obes Metab *15*, 503-512.

Pullen, T.J., Sylow, L., Sun, G., Halestrap, A.P., Richter, E.A., and Rutter, G.A. (2012). Overexpression of Monocarboxylate Transporter-1 (Slc16a1) in Mouse Pancreatic beta-Cells Leads to Relative Hyperinsulinism During Exercise. Diabetes *61*, 1719-1725.

Rodriguez-Diaz, R., Dando, R., Jacques-Silva, M.C., Fachado, A., Molina, J., Abdulreda, M.H., Ricordi, C., Roper, S.D., Berggren, P.O., and Caicedo, A. (2011). Alpha cells secrete acetylcholine as a non-neuronal paracrine signal priming beta cell function in humans. Nature Medicine *17*, 888-892.

Rorsman, P., and Ashcroft, F.M. (2018). Pancreatic beta-Cell Electrical Activity and Insulin Secretion: Of Mice and Men. Physiol Rev *98*, 117-214.

Rutter, G.A., Pullen, T.J., Hodson, D.J., and Martinez-Sanchez, A. (2015). Pancreatic beta-cell identity, glucose sensing and the control of insulin secretion. Biochem J *466*, 203-218.

Sanchez, P.K.M., Khazaei, M., Gatineau, E., Geravandi, S., Lupse, B., Liu, H., Dringen, R., Wojtusciszyn, A., Gilon, P., Maedler, K., et al. (2021). LDHA is enriched in human islet alpha cells and upregulated in type 2 diabetes. Biochem Biophys Res Commun *568*, 158-166.

Satija, R., Farrell, J.A., Gennert, D., Schier, A.F., and Regev, A. (2015). Spatial reconstruction of single-cell gene expression data. Nat Biotechnol *33*, 495-502.

Schuit, F., Van Lommel, L., Granvik, M., Goyvaerts, L., de Faudeur, G., Schraenen, A., and Lemaire, K. (2012). beta-cell-specific gene repression: a mechanism to protect against inappropriate or maladjusted insulin secretion? Diabetes *61*, 969-975.

Sdao, S.M., Ho, T., Poudel, C., Foster, H.R., De Leon, E.R., Adams, M.T., Lee, J.H., Blum, B., Rane, S.G., and Merrins, M.J. (2021). CDK2 limits the highly energetic secretory program of mature beta cells by restricting PEP cycle-dependent K(ATP) channel closure. Cell Rep *34*, 108690.

Segerstolpe, Å., Palasantza, A., Eliasson, P., Andersson, E.-M., Andréasson, A.-C., Sun, X., Picelli, S., Sabirsh, A., Clausen, M., Bjursell, M.K., et al. (2016). Single-Cell Transcriptome Profiling of Human Pancreatic Islets in Health and Type 2 Diabetes. Cell Metabolism *24*, 593-607.

Sekine, N., Cirulli, V., Regazzi, R., Brown, L.J., Gine, E., Tamarit-Rodriguez, J., Girotti, M., Marie, S., MacDonald, M.J., Wollheim, C.B., et al. (1994). Low lactate dehydrogenase and high mitochondrial glycerol phosphate dehydrogenase in pancreatic beta-cells. Potential role in nutrient sensing. Journal of Biological Chemistry *269*, 4895-4902.

Simpson, N.E., Khokhlova, N., Oca-Cossio, J.A., and Constantinidis, I. (2006). Insights into the role of anaplerosis in insulin secretion: A 13C NMR study. Diabetologia *49*, 1338-1348.

Spegel, P., Sharoyko, V.V., Goehring, I., Danielsson, A.P., Malmgren, S., Nagorny, C.L., Andersson, L.E., Koeck, T., Sharp, G.W., Straub, S.G., et al. (2013). Time-resolved metabolomics analysis of beta-cells implicates the pentose phosphate pathway in the control of insulin release. Biochem J *450*, 595-605.

Thorens, B., Sarkar, H.K., Kaback, H.R., and Lodish, H.F. (1988). Cloning and functional expression in bacteria of a novel glucose transporter present in liver, intestine, kidney, and beta-pancreatic islet cells. Cell *55*, 281-290.

van Gurp, L., Fodoulian, L., Oropeza, D., Furuyama, K., Bru-Tari, E., Vu, A.N., Kaddis, J.S., Rodriguez, I., Thorel, F., and Herrera, P.L. (2022). Generation of human islet cell type-specific identity genesets. Nat Commun *13*, 2020.

Wallace, M., Whelan, H., and Brennan, L. (2013). Metabolomic analysis of pancreatic beta cells following exposure to high glucose. Biochimica et Biophysica Acta (BBA) - General Subjects *1830*, 2583-2590.

Wang, Y.J., Schug, J., Won, K.J., Liu, C., Naji, A., Avrahami, D., Golson, M.L., and Kaestner, K.H. (2016). Single-Cell Transcriptomics of the Human Endocrine Pancreas. Diabetes *65*, 3028-3038.

bioRxiv preprint doi: https://doi.org/10.1101/2022.12.21.521364; this version posted December 21, 2022. The copyright holder for this preprint (which was not certified by peer review) is the author/funder, who has granted bioRxiv a license to display the preprint in perpetuity. It is made available under aCC-BY-NC 4.0 International license.

566 Xin, Y., Gutierrez, G.D., Okamoto, H., Kim, J., Lee, A.H., Adler, C., Ni, M., Yancopoulos, G.D.,
567 Murphy, A.J., and Gromada, J. (2018). Pseudotime Ordering of Single Human beta-Cells
568 Reveals States of Insulin Production and Unfolded Protein Response. Diabetes.
569 Zaborska, K.E., Dadi, P.K., Dickerson, M.T., Nakhe, A.Y., Thorson, A.S., Schaub, C.M., Graff,
570 S.M., Stanley, J.E., Kondapavuluru, R.S., Denton, J.S., et al. (2020). Lactate activation of
571 alpha-cell KATP channels inhibits glucagon secretion by hyperpolarizing the membrane
572 potential and reducing Ca(2+) entry. Mol Metab *42*, 101056.
573 Ždralević, M., Brand, A., Di Ianni, L., Dettmer, K., Reinders, J., Singer, K., Peter, K., Schnell,
574 A., Bruss, C., Decking, S.-M., et al. (2018). Double genetic disruption of lactate
575 dehydrogenases A and B is required to ablate the “Warburg effect” restricting tumor growth to
576 oxidative metabolism. Journal of Biological Chemistry *293*, 15947-15961.

577
578

bioRxiv preprint doi: https://doi.org/10.1101/2022.12.21.521364; this version posted December 21, 2022. The copyright holder for this preprint (which was not certified by peer review) is the author/funder, who has granted bioRxiv a license to display the preprint in perpetuity. It is made available under aCC-BY-NC 4.0 International license.

FIGURES AND FIGURE LEGENDS

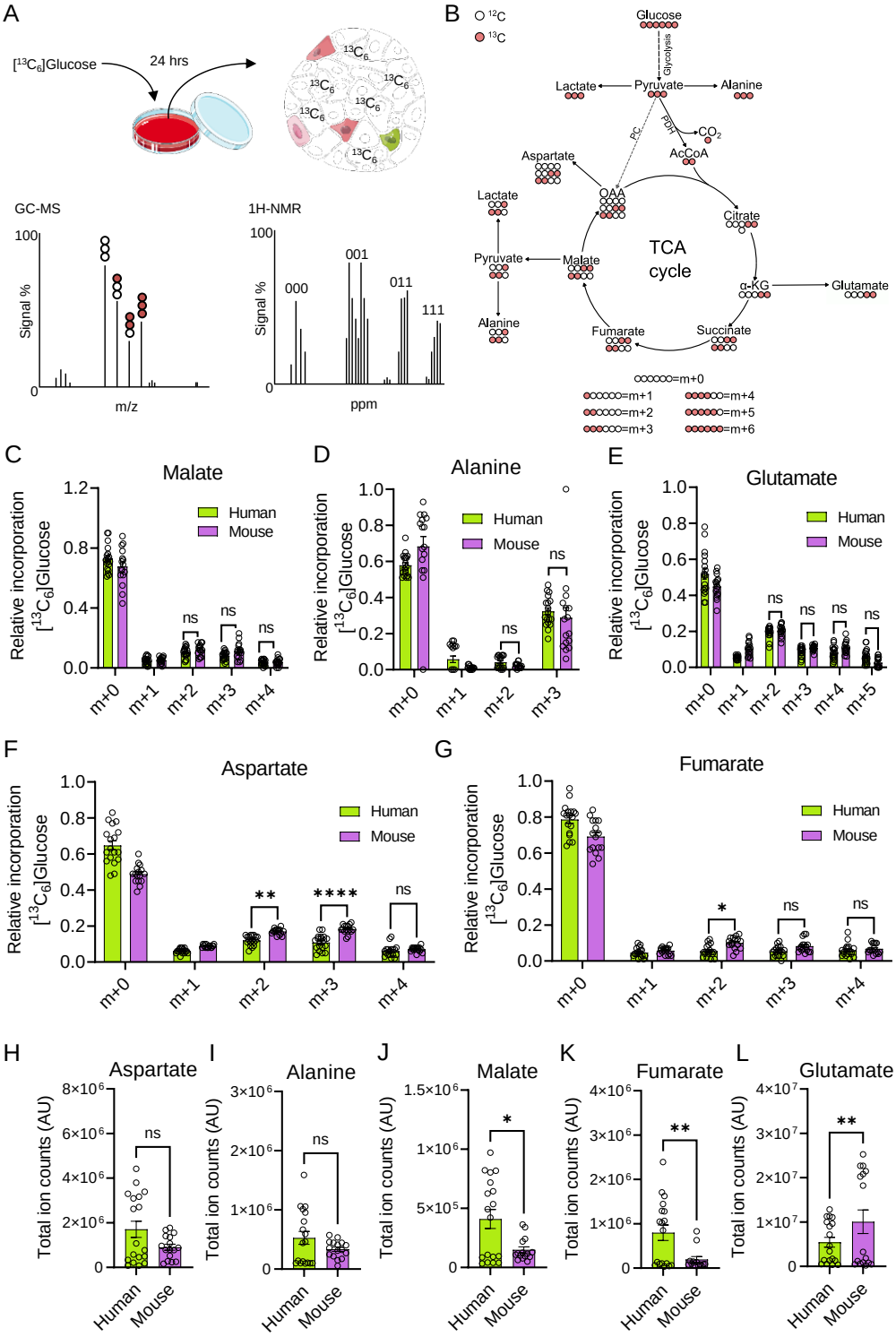

Figure 1: MID analysis of glucose fate in human and mouse islets. A) Schematic showing GC-MS and ^{1}H-NMR-based $^{13}C_6$ glucose-tracing protocol in primary islets. **B)** Schematic showing mass isotopomer distribution (MID) analysis of $^{13}C_6$ glucose-tracing data. **C-E)** MID analysis showing similar incorporation of ^{13}C from $^{13}C_6$ glucose into malate (C), alanine (D) and glutamate (E) in human and mouse islets. **F, G**) MID analysis showing increased incorporation of ^{13}C from $^{13}C_6$ glucose into m+2 aspartate (F), and m+2 and m+3 fumarate (G) in mouse compared to human islets. **H, I)** Total amount of extracted aspartate (H) and alanine (I) is similar in human and mouse islets. **(J-L)** Total amount of extracted malate (J) and

bioRxiv preprint doi: https://doi.org/10.1101/2022.12.21.521364; this version posted December 21, 2022. The copyright holder for this preprint (which was not certified by peer review) is the author/funder, who has granted bioRxiv a license to display the preprint in perpetuity. It is made available under aCC-BY-NC 4.0 International license.

589 fumarate (K) is decreased in mouse relative to human islets, whereas glutamate (L) is
590 increased. For all data, n = 18 independent replicates from 9 human donors; n = 10 islet
591 preparations from 15 animals. C-G were analyzed using two-way ANOVA and Sidak's post-
592 hoc test. H-L were analyzed using Welch's test. Bar graphs show individual datapoints and
593 mean ± SEM. AU = arbitrary unit.
594
595

bioRxiv preprint doi: https://doi.org/10.1101/2022.12.21.521364; this version posted December 21, 2022. The copyright holder for this preprint (which was not certified by peer review) is the author/funder, who has granted bioRxiv a license to display the preprint in perpetuity. It is made available under aCC-BY-NC 4.0 International license.

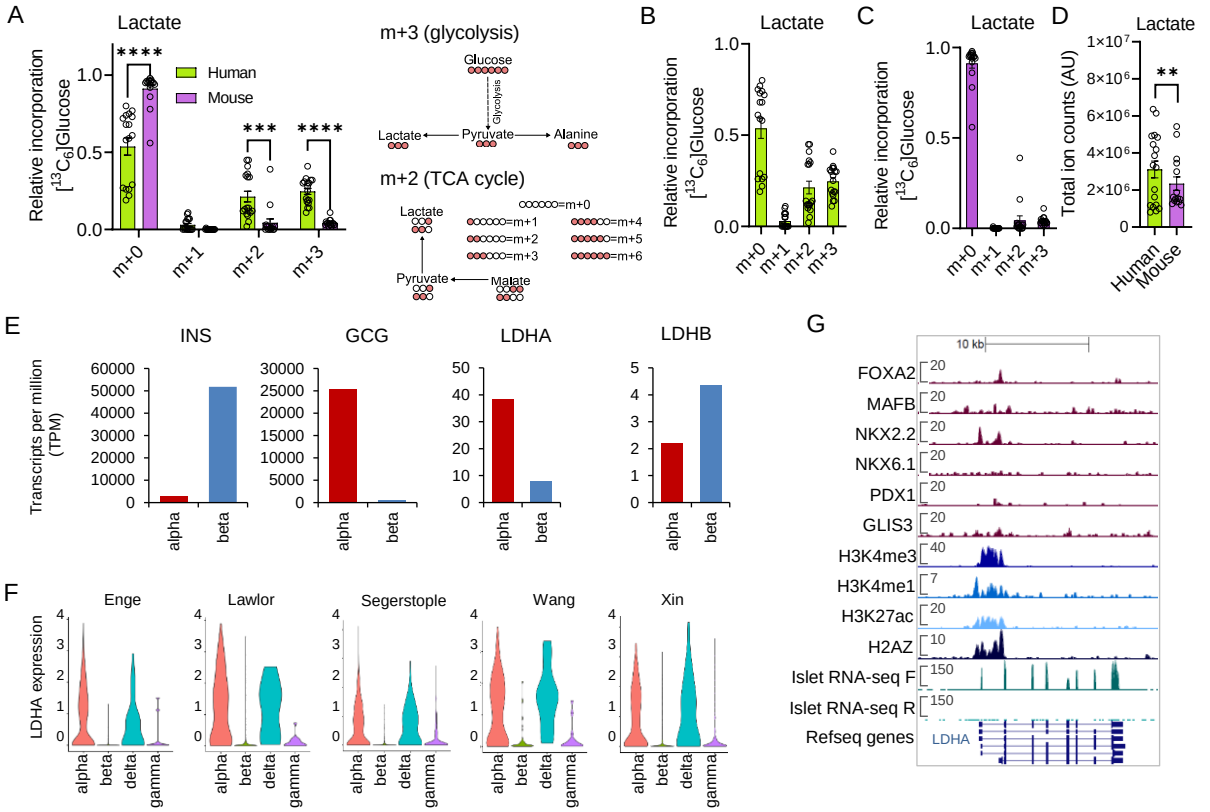

Figure 2: Human and mouse islets convert pyruvate to lactate. A-C) MID analysis shows detectable glucose incorporation into m+2 (TCA cycle) and m+3 (pyruvate conversion) lactate, with more accumulation in human (A, B) versus mouse (A, C) islets. **D)** Total lactate production is higher in human compared to mouse *islets*. **E)** Normalized mRNA levels (transcripts per million, TPM) for *INS*, *GCG*, *LDHA* and *LDHB* genes in fluorescent-activated cell-sorted (FACS) alpha and β cell samples (re-analysis of data from (Arda et al., 2016)). **F)** Normalized LDHA expression in , β, δ and γ cells from five independent human islet single cell RNA-sequencing experiments (Enge et al., 2017; Lawlor et al., 2017; Segerstolpe et al., 2016; Wang et al., 2016; Xin et al., 2018). Data from each study was subjected to re-assignment of cell identity based upon strict criteria (see Methods). **G)** Genome browser snapshot of transcription factor binding, histone modification (ChIP-seq, targets as indicated) and RNA-sequencing experiments performed on human islets (Akerman et al., 2017). Scales represent RPKM. For A-D, n = 18 independent replicates from 9 human donors; n = 10 islet preparations from 15 animals. A was analyzed using two-way ANOVA and Sidak's post-hoc test. D was analyzed using Welch's test. Bar graphs show individual datapoints and mean ± SEM. AU = arbitrary unit.

bioRxiv preprint doi: https://doi.org/10.1101/2022.12.21.521364; this version posted December 21, 2022. The copyright holder for this preprint (which was not certified by peer review) is the author/funder, who has granted bioRxiv a license to display the preprint in perpetuity. It is made available under aCC-BY-NC 4.0 International license.

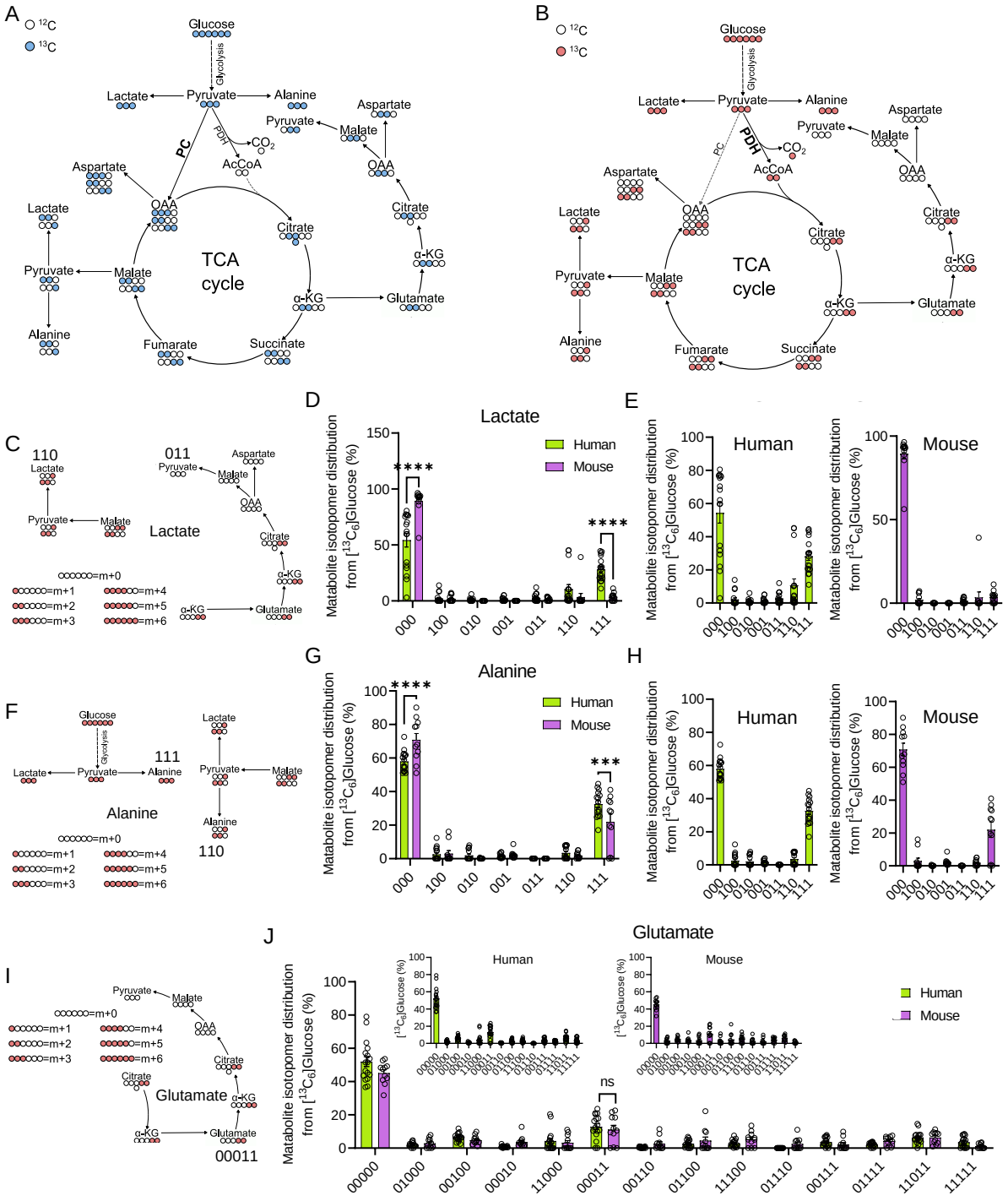

Figure 3: Incorporation of ^{13}C from $^{13}C_6$ glucose into TCA cycle metabolites through PDH and PC. **A)** White and blue circles, respectively, show the incorporation of ^{12}C and ^{13}C into TCA cycle metabolites arising from metabolism of pyruvate by PC. **B)** White and red circles, respectively, represent ^{12}C and ^{13}C atoms as incorporated from $^{13}C_6$ glucose into the TCA cycle through the conversion of pyruvate to acetyl-CoA by PDH. **C-E)** $Lactate_{000}$, $lactate_{111}$ and $lactate_{110}$ are the most abundant isotopomers (C) in both humans and mice (D), although the incorporation of ^{13}C from $^{13}C_6$ glucose into $lactate_{111}$ is significantly higher in human than mouse islets (D, E). **F-H)** ^{13}C incorporation into alanine isotopomers (F) is similar in human and mouse islets (G), with $alanine_{111}$ being the most represented labeled isotopomer (G, H). **I, J**) The distribution of labeling patterns for glutamate (I) are similar in human and

bioRxiv preprint doi: https://doi.org/10.1101/2022.12.21.521364; this version posted December 21, 2022. The copyright holder for this preprint (which was not certified by peer review) is the author/funder, who has granted bioRxiv a license to display the preprint in perpetuity. It is made available under aCC-BY-NC 4.0 International license.

626 mouse islets (J), with glutamate$_{00011}$ being the most abundant labeled isotopomer in both
627 species (J). For all data, n = 16-17 islet preparations, 9 human donors and n = 7-8 islet
628 preparations, 12-15 animals. Data were analyzed using 2-way ANOVA and Sidak's post-hoc
629 test. Bar graphs (scatter plot) show mean ± SEM. Bar graphs show individual datapoints and
630 mean ± SEM. AU = arbitrary unit.
631
632

bioRxiv preprint doi: https://doi.org/10.1101/2022.12.21.521364; this version posted December 21, 2022. The copyright holder for this preprint (which was not certified by peer review) is the author/funder, who has granted bioRxiv a license to display the preprint in perpetuity. It is made available under aCC-BY-NC 4.0 International license.

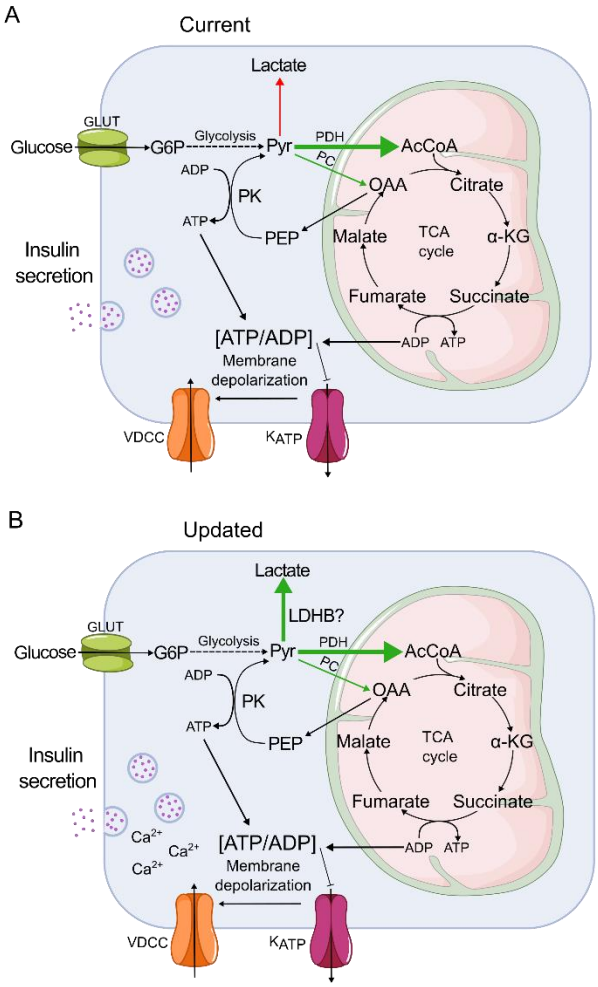

Figure 4: Schematic showing pyruvate management in human and mouse islets. A) In the current view (top) of β cell metabolism, glycolytically-derived pyruvate enters the TCA through the actions of pyruvate dehydrogenase (PDH) and pyruvate carboxylase (PC). The PEP cycle and extra-mitochondrial ADP makes a disproportionate contribution to K_{ATP} channel regulation and the triggering phase of insulin secretion. Alternative fates for pyruvate (i.e. production of lactate) are suppressed. **B)** The high-resolution view of β cell metabolism reveals that some pyruvate is converted to lactate, before entering into the TCA predominantly through the action of pyruvate dehydrogenase, likely to maintain REDOX and β cell housekeeping functions.

bioRxiv preprint doi: https://doi.org/10.1101/2022.12.21.521364; this version posted December 21, 2022. The copyright holder for this preprint (which was not certified by peer review) is the author/funder, who has granted bioRxiv a license to display the preprint in perpetuity. It is made available under aCC-BY-NC 4.0 International license.

647 **Table 1: Human islet donor characteristics.** BMI, body mass index. IFG, impaired fasting
648 glucose.

Unique identifier	Age group (years)	Gender	BMI (Kg/m^2)	Glycemia (mmol/L)* HbA1C (%)	History of diabetes**	Islet purity (%)	Islet culture duration (h)	Country of origin
HP1404	50-55	♂	29.4	7.8 mmol/L	No	80	18	Italy
HP1406	60-65	♂	26.1	N/A	No	90	96	Italy
HP1408	55-60	♀	19.0	N/A	No	90	18	Italy
HP1416	60-65	♂	31.1	N/A	No but IFG	75	20	Italy
HP1419	55-60	♂	22.8	7.3 mmol/L	No	90	18	Italy
HP1431	60-65	♀	26.9	8.0 mmol/L	No	90	18	Italy
HI1117	45-50	♂	24.0	5.4%	No	80	N/A	France
HI1120	50-55	♂	29.5	5.7%	No	90	N/A	France
HI1121	60-65	♂	32	5.5%	No	90	N/A	France

649